RSC Advances

This article can be cited before page numbers have been issued, to do this please use: S. S. Boxi and S. Paria, *RSC Adv.*, 2015, DOI: 10.1039/C5RA03421C.

ROYAL SOCIETY OF CHEMISTRY

www.rsc.org/advances

View Article Online
DOI: 10.1039/C5RA03421C

Visible Light Induced Enhanced Photocatalytic Degradation of Organic Pollutants in Aqueous Media Using Ag Doped Hollow TiO_2 Nanospheres

Siddhartha Sankar Boxi, Santanu Paria*

Interfaces and Nanomaterials Laboratory, Department of Chemical Engineering, National Institute of Technology, Rourkela 769 008, Orissa, India.

Abstract:

The silver doped hollow TiO_2 (Ag-h-TiO_2) nanoparticles were synthesized by a sacrificial core (AgBr) method. The Ag doping and the core removal was done simultaneously during the dissolution of the core in $(NH_4)OH$ solution. The mean particle size of synthesized Ag-h-TiO_2 nanoparticles is 17.76 ± 2.85 nm with the wall thickness ~2.5 nm. The hollow structured nanoparticles have 103.2 m^2/g more specific surface area compared to that of solid TiO_2 nanoparticles. The suitability of this synthesized hollow nanoparticles as photocatalyst were tested for the photocatalytic degradation of three important different classes of organic compounds such as nitrobenzene (NB), metronidazole (MTZ) antibiotic, and methylene blue dye (MBD) in aqueous solution under irradiation of visible light. Photodegradation studies show there is a significant enhancement of the degradation efficiency of the TiO_2 after the hollow structure formation and silver doping. The recycling tests of the catalysts show only ~ 10% decrease in efficiency for NB and MTZ degradation after sixth cycle of reuse. The light emission capacity in terms of quantum yield (QY) is enhanced by 18.7% for Ag-h-TiO_2 than that of pure TiO_2 nanoparticles.

Key words: Hollow nanoparticles, Ag doped TiO_2, photodegradation, visible light, quantum yield.

* To whom correspondence should be addressed. E–mail: santanuparia@yahoo.com, or sparia@nitrkl.ac.in; Fax: +91 661 246 2999

View Article Online
DOI: 10.1039/C5RA03421C

1. Introduction

Metal oxide semiconductor nanoparticles play an important role in different areas of science and engineering such as photo catalysis, [1–3] solar cells, [4–6] Li-ion batteries, [7,8] piezoelectric devices, [9,10] fuel cells, [11] sensors, [12,13] and so on. The photo catalytic degradation of organic pollutants is considered as one of the advanced environmental remediation process in recent years over the conventional processes such as membrane filtration, adsorption. Among several metal oxide semiconductor nanoparticles TiO_2 is one of the promising photocatalysts because of its relatively higher efficiency, low toxicity, long term stability, low cost, photoinduced strong oxidation activity properties. [14–16] However, the application of pure TiO_2 as a photocatalyst is limited in visible light because of its high band gap (3.03 eV for rutile and 3.18 eV for anatase). Because of this reason, the development of visible light induced TiO_2 photocatalyst with higher efficiency is highly essential to make the industrial process more feasible and economic. Since the reduction of band gap enhance the photocatalytic activity of a photocatalyst under visible light, significant efforts have been made till now to dope different elements into the TiO_2 host lattices such as, Fe, [17,18] Mn, [19] Mg, [20] Cr, [21] Co, [22] Sn, [23] Sm, [24] Nd, [25] and so on. In addition to the band gap of a photocatalyst, the surface area is also extremely important to enhance the activity of a catalyst. In this regard, TiO_2 with different morphologies such as nanowires, [26] nanotubes, [27] nanorods [28] have been studied. More advanced material like hollow nanoparticles along with doping have attracted considerable interests because of its larger surface area along with some important properties, such as low density, good surface permeability and high light-harvesting efficiencies, [29–32] The TiO_2 photocatalysts are not only used for the remediation of contaminated water but also useful in air purification, [33] cathodic catalyst for low-cost fuel cell. [34] Some studies are also available on hollow TiO_2 nanoparticles doped with different elements such as Nd, [35] N and Ce, [36] Sn, [37] Bi, [38] in all these studies the C was used as the core and it was removed by calcination. The other template such as polystyrene was used for Sm^{3+} doped hollow TiO_2 structure. [39] Sulfur doped hollow sphere TiO_2 was also synthesized by our group, where S was doped during the removal of the sacrificial S core. [40] Considering catalytic properties of TiO_2, incorporation of noble metal like Ag to hollow TiO_2 structure is important because of its unique characteristics in resonant collective oscillations of the conduction electrons by electromagnetic radiation and the localized surface plasmon resonance (SPR). [41,42] Since nanoscale silver has good antibacterial property, [43,44] Ag doped TiO_2 nanoparticles also show similar property. [45–47] Silver-TiO_2 composite hollow nanoparticles was reported by template free method [48] and PSA latex templated method [49] as a visible light active photocatalyst.

View Article Online
DOI: 10.1039/C5RA03421C

Recently, Ag and AgCl doped TiO_2 hollow nanoparticles were synthesized using polystyrene particles as template for getting a visible light active photocatalyst. [50]

It has been noted from most of the literature that the doped hollow structure was formed after removing the core, and the doping was achieved in the presence of some extra precursor. However, a single step method for the core removal and doping could make the process simple.

As mentioned before, a significant fraction of research activities is going on environmental remediation of organic pollutants using TiO_2 nanoparticles. The main advantage of this process over the other conventional separation processes is toxic pollutants can be converted to useful or nontoxic compounds. Different classes of organic compounds such as aromatics (benzo compounds, phenolic compounds, naphthalene, trinitrotoluene, etc), phermaceutical products (antibiotics, antipyretic etc.), dyes (synthetic dyes, reactive dyes, azo dyes, basic cationic dyes etc.), some volatile organic compounds (formaldehyde, methylene chloride, ethylene glycol, etc) can be degraded using this catalysts. The benzo compounds such as nitrobenzene are highly toxic organic compound mainly used for the production of aniline, paper and pulp, pesticides, dyes, explosives, cosmetics, pharmaceuticals, and so on. [51–53] The long term exposure of nitrobenzene to the environment, even at low concentration, causes risks to human, such as liver or kidney damage, lung irritation, increase heart rate, skin problem, vomiting, etc. Therefore, removal of nitrobenzene from the environment is a major concern. Degradation of nitrobenzene in effluent water is difficult by conventional chemical method because of the nitro group which has strong electron withdrawing property and inhibits its oxidation, or by biological method because of its toxic and mutagenic effect on the biological systems. [54,55] Apart from aromatic compounds, the presence of pharmaceutical products for instance antibiotics in the environment, even at low concentrations, causes the growth of antibiotic-resistant bacteria [56,57] and creates microbial population, [58,59] which may cause of ineffectiveness of the present forms of treatment and major epidemics. Metronidazole (MTZ) is one such type of antibiotic which is primarily used for the infectious diseases caused by anaerobic bacteria and protozoa. Complete removal of metronidazole from the environment by conventional method is difficult because of its low degradability and high solubility in water. Dye contamination is another critical environmental problem and addressed by several researchers till now. The sources of synthetic dyes in wastewater are from different industries such as, textile, dye and dye intermediates, paper and pulp, printing, colour photography, petroleum industries, and so on. [60,61] Continuous discharge of dye-bearing effluents from these industries into natural stream

View Article Online
DOI: 10.1039/C5RA03421C

and rivers poses severe environmental problems as toxic to useful microorganisms, aquatic life, and human beings. So, suitable and efficient techniques are highly essential for the treatment of these industrial effluents.

In this study Ag-h-TiO_2 nanoparticles were synthesized through a sacrificial core technique using AgBr as the core. The core was removed under a mild condition by dissolving in ammonium hydroxide solution, and the silver doping was also achieved during the dissolution of the core without any addition extra dopant precursor. After Ag doping, pure anatase phase TiO_2 particles were obtained even after heating at 450 °C. The hollow structure nanoparticles have higher surface area (198.3 m^2/g) compared to solid TiO_2 nanoparticles (95.1 m^2/g) and hollow structures reported by other researchers. [62–66] To test the photocatalytic activity of the developed nanoparticles towards three important organic compounds such as nitrobenzene (NB), metronidazole (MTZ), and methylene blue dye (MBD) degradation studies were conducted with low catalyst dose and high initial MTZ concentration compared to the studies reported till now. The obtained TiO_2 particles are having low band gap, anatase phase, high surface area, good crystallinity, and efficient visible light induced photocatalytic property to degrade important organic compounds such as nitrobenzene, antibiotic, and dye.

2. Materials and Methods

2.1 Materials

Reagent-grade silver nitrate (99.9%) and potassium bromide (99.3%) were purchased from Rankem. Anionic surfactant sodium dodecyl benzene sulphonate (SDBS) (technical grade, Cat No. 28995-7) and titanium (IV) butoxide ($Ti[O(CH_2)_3CH_3]_4$ or TOBT, 97%) were obtained from Sigma Aldrich. Ammonium hydroxide (25%), nitric acid (69% GR), cyclohexane, and methylene blue dye were bought from Merck. Nitrobenzene was provided by Nice Chemicals Pvt. Ltd. Metronidazole was supplied by J B Chemicals & Pharmaceuticals Ltd. All the chemicals were used as it was received without any further purification. Ultrapure water of 18.2 MΩ.cm resistivity and pH 6.4–6.5 was used for all the experiments.

2.2 Methods

A sol-gel method was followed for the synthesis of silver doped hollow TiO_2 nanoparticles using AgBr as the sacrificial core. The AgBr nanoparticles were synthesized in aqueous

View Article Online
DOI: 10.1039/C5RA03421C

SDBS media according to our previous reported study. [67] The concentrations of both $AgNO_3$ and KBr were maintained at 0.1 mM. After the formation of AgBr NPs the suspension was sonicated using a bath sonicator for 20 min, TBOT was then added slowly under constant stirring condition for uniform coating on the core surface. After 5 minutes of addition of TBOT, HNO_3 was added to maintain the pH of ~2 and kept for 35 min under stirring condition. The $AgBr/TiO_2$ core/shell nanoparticles were then separated by centrifugation at 25,000 rpm for 20 min and washed thrice with ethanol and water mixture (2:1, v/v). Then the particles were dipped in ammonium hydroxide solution (2.5 mM) for 48 hrs for the dissolution of AgBr core. The particles were separated and calcined at 450°C for 2 hrs to improve the crystallinity. For quantum yield (QY) calculation of Ag-h-TiO_2 NPs, phenol was used as a reference (QY=0.14).

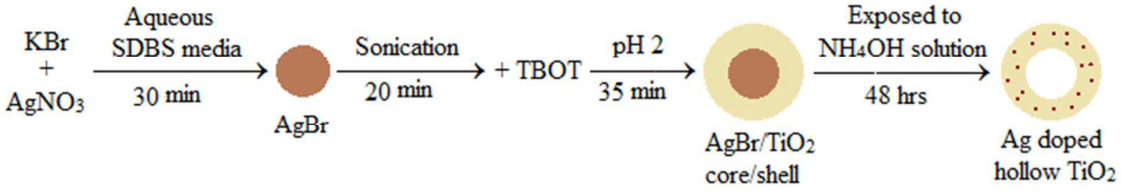

Scheme 1. Schematic presentation for the formation of Ag-h-TiO_2 nanoparticles.

2.3 Particles characterization

The particle size was measured initially by dynamic light scattering (DLS) using a Malvern Zeta Size analyzer, (Nano ZS). The crystallinity of synthesized particles was characterized using powder X-ray diffraction (XRD) (Philips, PW 1830 HT) with scanning rate of 0.01°/s in the 2θ range from 20° to 70°. The size and shape of the particles were observed under a field emission scanning electron microscope (FE-SEM) (FEI, Nova NanoSEM NPE212) and transmission electron microscope (TEM) (FEI, Tecnai S-twin). The elemental composition of the sample was analyzed by energy-dispersive X-ray spectroscopy (EDX) (Oxford Instruments, model X-sight) attached to the HR-TEM (JEOL, JEM 2100). The light absorbance and luminescence properties were also characterized by UV–vis–NIR Spectroscopy (Shimadzu, UV-3600) and fluorescence spectroscopy (Hitachi, F-7000) respectively. Fourier transform infrared spectroscopy (FT-IR) was carried out using an FT-IR (Thermo Fisher Scientific, Nicolet iS10). The chemical composition of the samples and the valence states of various elements were analyzed by X-ray photoelectron spectroscopy (XPS, ULVAC-PHI, Inc., PHI 5000 Versa Probe II.). The surface area of the nanoparticles was measured by Brunauer–Emmett–Teller (BET) technique (Quantachrome, USA).

View Article Online
DOI: 10.1039/C5RA03421C

2.4 Photocatalytic degradation

The photocatalytic activity of the synthesized catalyst was tested by the degradation of NB, MTZ antibiotic, and MBD in aqueous solutions. For nitrobenzene degradation the initial concentration of nitrobenzene and catalyst dose were maintained 61.5 mg/L and 0.05 g/L. For MTZ degradation the initial concentration of the MTZ solution was maintained to 15 mg/L for all experiments and the catalyst concentration was 0.5 g/L. The degradation studies were conducted in a photoreactor equipped with a 125 W high pressure mercury vapour lamp (λ=435.8 nm, light intensity 27000 LUX, light energy 56 ± 2 w/m^2) placed about 12 cm away from the solution. The solutions were stirred continuously using a magnetic stirrer. Prior to each test, the lamp was turned on 10 min before in order to get a maximum light intensity. The samples were magnetically stirred for 20 min in the dark to allow physical adsorption equilibrium of NB, MTZ, and MBD on the catalyst surface. Then the suspension was exposed to visible light irradiation under constant stirring condition. The sample was then taken out and centrifuged to remove the nanoparticles after each 20 min interval for MTZ and 30 min interval for NB and MBD degradation. Then the concentration of the NB, MTZ, and MBD solution were analyzed using a UV-Vis-NIR Spectrophotometer at its maximum absorbance wavelength of λ = 267, 320, and 661 nm for NB, MTZ, and MBD, respectively. The cyclic degradation test was conducted to check the reusability of the photocatalyst. After each cycle of degradation the catalyst was separated by centrifugation and was used for the next cycle of degradation without any pre-treatment. The intermediate and final degraded products during nitrobenzene degradation were analyzed by liquid chromatography-mass (LC-MS) (Flexar SQ 300 MS, Perkin Elmer). The sample was extracted with cyclohexane and 70% water/30% acetonitrile (v/v) mobile phase was used for the analysis.

3. Results and discussion

3.1 Synthesis of hollow TiO_2 particles

The hollow particles were synthesized by the templated sacrificial core method using AgBr as a core. In aqueous media the surface charge of AgBr nanoparticles is -15 to -25 mV. Addition of anionic surfactant (SDBS) makes the surface charge of AgBr more negative (-47.8 mV). The surface charge of TiO_2 nanoparticles is positive, so, it is expected that the TiO_2 will favourably coat on the AgBr core surface because of the electrostatic attraction. When ammonium hydroxide solution was added to the particle suspension, AgBr would try

View Article Online
DOI: 10.1039/C5RA03421C

to dissolve in ammonium hydroxide through the formation of soluble complex according to equation 1. During the dissolution of AgBr, there is a chance of doping of Ag on TiO_2 shell.

$$AgBr\ (s) + 2\ NH_3\ (aq) \rightarrow Ag(NH_3)_2^+(aq) + Br^- \quad (1)$$

3.2 Characterization of particles by UV-Vis spectroscopy

UV-Vis spectroscopic study was done to investigate the light absorption property of the nanoparticles, and the results are presented in Figure 1. The Figure shows that the sharp peak of pure AgBr is present in the UV region (237 nm), and it disappears after the coating of external shell layer of TiO_2 on AgBr. Pure TiO_2 is having major absorption below 350 nm wavelength, and there is no absorption in the visible region, this is because of its high energy band gap (3.2 eV). However, the UV-Vis spectra of Ag-h-TiO_2 nanoparticles show a significant absorption in 300-650 nm wavelength range. The shifting of absorbance in the visible range is attributed to the fact of lowering of the band gap of the obtained nanoparticles because of doping of Ag. In addition, noteworthy to mention that, the absorption intensity of Ag-h-TiO_2 is higher compared to that of pure solid TiO_2 in both UV as well as in visible regions. The increase in absorbance is also attributed to the fact of porous hollow structure and formation of shell layer by the deposition of small particles. The band gap energy was calculated using the equation $E_g = 1239.8/\lambda$ [68] to support the above fact, where E_g is the band gap (eV) and λ is the wave length (nm) of the absorption edges in the UV –Vis spectrum. It has been found that the calculated band gaps are 2.69 and 3.29 eV for AgBr and TiO_2, which are in good agreement with the reported values of 2.7 eV [69] and 3.28 eV [70] respectively, whereas, 2.48 and 2.25 eV for AgBr/TiO_2 and Ag-h-TiO_2 nanoparticles respectively. Since the band gap of the TiO_2 is reduced after the formation of doped hollow structure, it is expected to be useful as good photocatalyst under the visible light irradiation, dye sensitized solar cells, or other electrochemical applications.

View Article Online
DOI: 10.1039/C5RA03421C

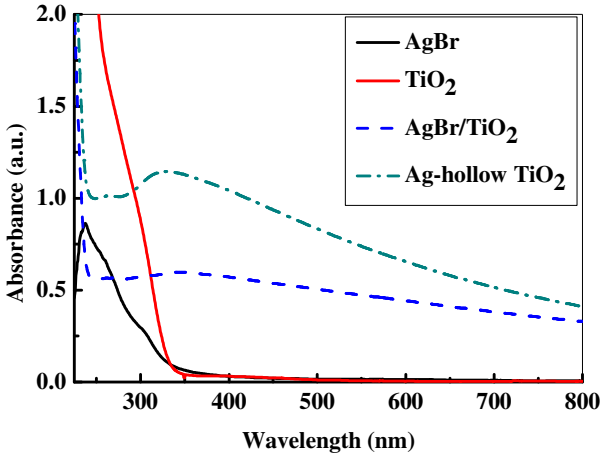

Figure 1. UV –Vis spectra of as synthesized AgBr, TiO_2, AgBr/TiO_2, and Ag-h-TiO_2 nanoparticles.

3.3 Characterization of particles by XRD

The crystallographic phases of the nanoparticles were identified by XRD technique. The diffraction patterns of all particles are presented in Figure 2. For pure AgBr, the XRD pattern displays peaks at 2θ value of 26.6, 30.9, 44.3, 55.2, 64.5, and 73.3° corresponding to the planes (111), (200), (220), (222), (400), and (420) of cubic structure (JCPDS card no.79-0149). For pure TiO_2, the anatase peaks were obtained at 2θ value of 25.1, 36.5 and 62.3° corresponding to the planes (101), (103), and (204) (JCPDS card no.71-1169). The peaks rutile phase were obtained at 2θ values of 27.3, 54.1, and 68.6° corresponding to the planes (110), (211), and (301) (JCPDS card no.76-0319). For AgBr/TiO_2 core/shell nanoparticles the XRD pattern shows the peaks of both AgBr and TiO_2, but the peak intensity of AgBr is reduced and that of TiO_2 becomes more dominant mainly because of TiO_2 coating. For Ag-h-TiO_2 NPs the TiO_2 anatase peaks (2θ) were obtained at 25.6, 37.4, 48.6, and 63.2° corresponding to the planes of (101), (103), (200), and (204) (JCPDS card no. 75-1537) with the peaks of elemental silver at 2θ values of 44.3 and 64.7, corresponding to the planes (200) and (220) (JCPDS card no.03-0931) respectively. Additionally, another important observation is the rutile peak at 2θ = 27.3° is absent in the hollow structure, while compare with pure TiO_2 NPs. The XRD analysis also shows that the anatase TiO_2 peak (2θ) of (101) plane shifts from 25.1° to 25.6° after the formation of hollow structure, which attributed to the silver doping to TiO_2 lattices.

View Article Online
DOI: 10.1039/C5RA03421C

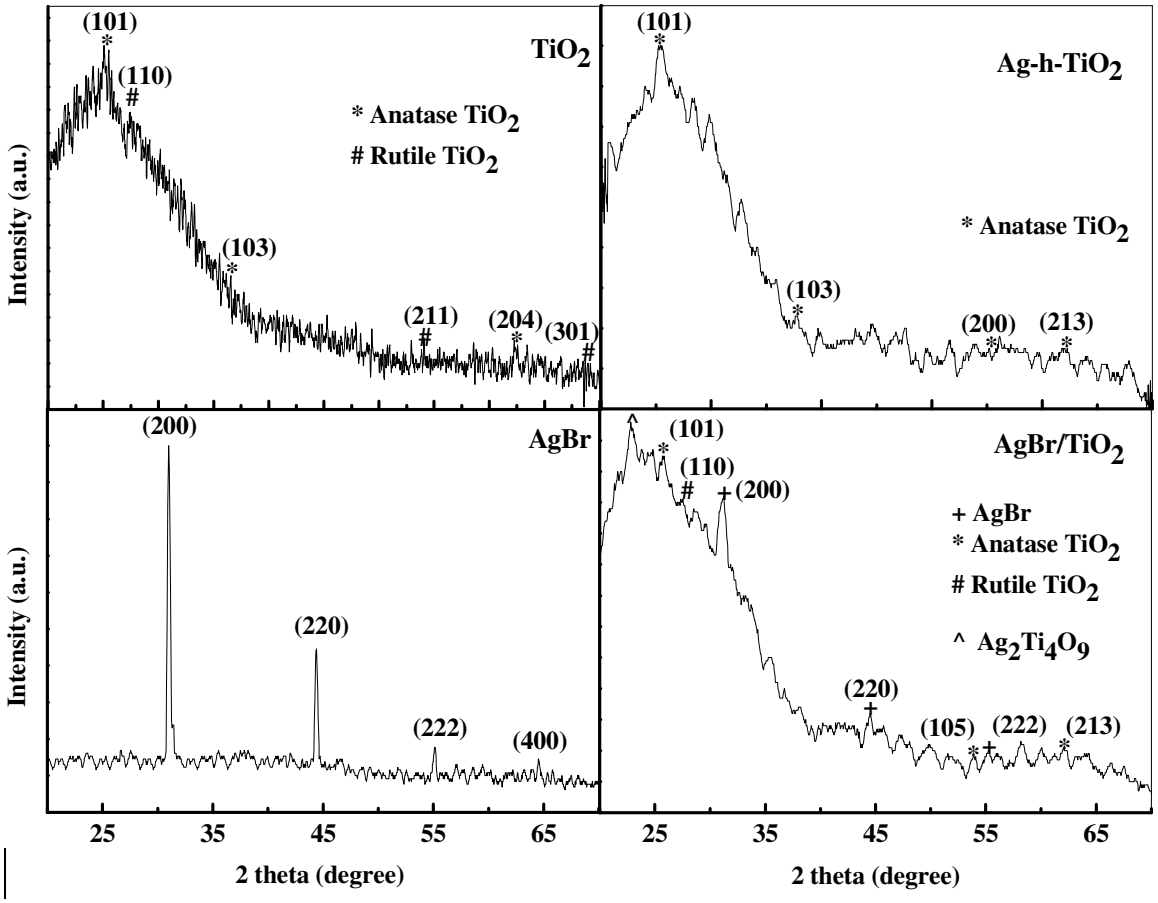

Figure 2. The X-ray diffraction patterns of AgBr, TiO_2, AgBr/TiO_2 core/shell, and Ag-h-TiO_2 nanoparticles.

3.4 Characterization of particles by TEM and FE-SEM

The Figure 3a shows the TEM image of AgBr/TiO_2 core/shell nanoparticles before expose to ammonium hydroxide solution. The contrast difference between the core and shell in the image indicates the formation of core/shell structure. The particles are spherical in shape, and the size distribution is plotted in Figure 3c which indicates the mean particle size of 17.86 ± 2.46 nm and the shell thickness is ~ 2.5 nm. The TEM image of AgBr/TiO_2 core/shell particles after dissolution in ammonium hydroxide solution is presented in Figure 3b. The particle size distribution is plotted in Figure 3d which shows mean particle size of 17.76 ± 2.85 nm, which is almost same as it was before the dissolution. However, the average particle size obtained by DLS measurement (S1, Supporting Information) was comparatively larger (20.79 nm) than that obtained by TEM measurement, this might be because of the adsorbed surfactant layer and hydrated water molecules [67]. The FE-SEM image (inset Figure 3b and

View Article Online
DOI: 10.1039/C5RA03421C

S2, Supporting Information) clearly shows some of the broken hollow spheres. The TEM image of single contrast indicates the removal of core. So, the TEM and FE-SEM images confirm the formation of hollow TiO_2 particles after treatment with ammonia solution. The high resolution TEM image of Ag-h-TiO_2 nanoparticles (Figure 4a) shows lattice fringes spacing of 0.353 nm corresponding to the (101) plane for anatase phase TiO_2 (JCPDS card no. 75-1537) previously confirmed by XRD. But there is no lattice fringe of rutile TiO_2 or Ag, which confirms 100% anatase phase of TiO_2 and no surface deposition of Ag. The Figure 4b shows the selected area electron diffraction (SAED) pattern of the hollow particle by focusing the electron beam on a single particle. The ring like diffraction pattern is indexed to (101) and (200) planes of TiO_2 together with (200) diffraction of silver, which confirms the presence of silver inside the crystal structure of TiO_2 nanoparticles. The EDX in Figure 4c further confirms the presence of silver, titanium, and oxygen atoms. Some extra peaks of Cu and C are mainly from TEM grids.

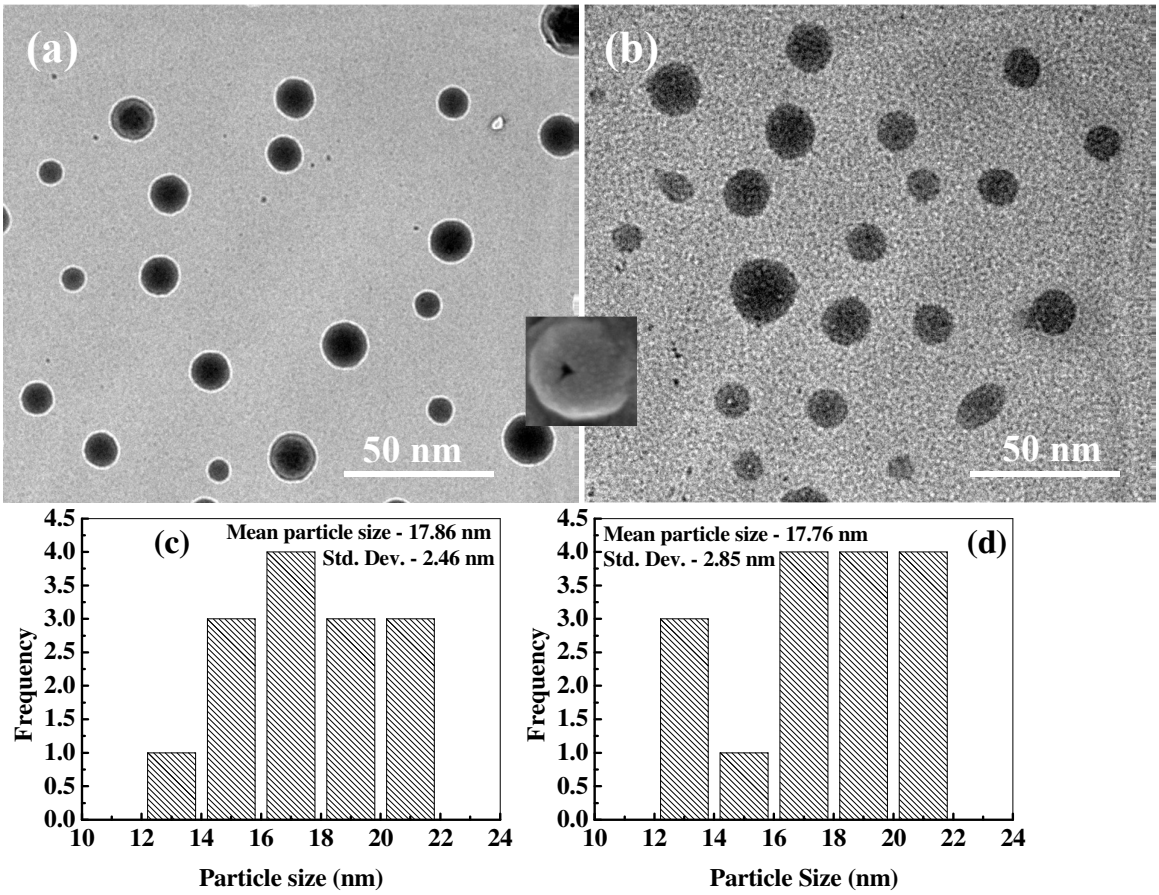

Figure 3. TEM images of (a) AgBr/TiO_2 core/shell, and (b) Ag-h-TiO_2 hollow nanoparticles, inset shows FE-SEM image of a hollow broken particle (more hollow particles are shown in

View Article Online
DOI: 10.1039/C5RA03421C

Figure S2). Particle size distributions of (c) AgBr/TiO_2 core/shell, and (d) Ag-h-TiO_2 nanoparticles.

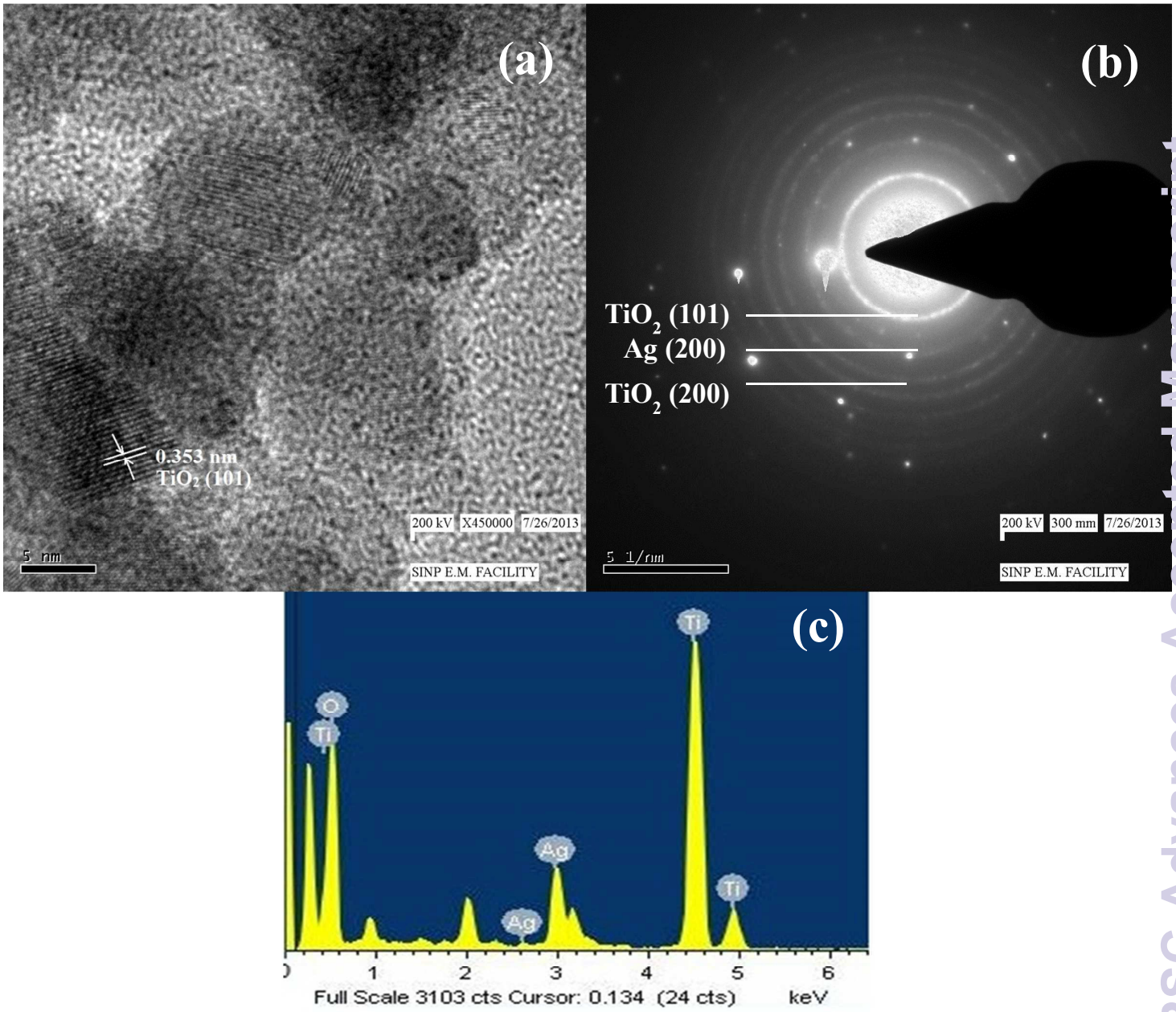

Figure 4. (a) HR-TEM image (b) SAED pattern, and (c) EDX pattern of Ag-h-TiO_2 nanoparticles.

3.5 Characterization of particles by XPS

View Article Online
DOI: 10.1039/C5RA03421C

For the further confirmation of the surface composition and the chemical states of Ag-h-TiO_2 nanoparticles, XPS analysis was carried out. The high resolution XPS spectra of Ag (3d), Ti (2p) and O (1s) are presented in Figure 5. The XPS peak at 462.9 eV corresponds to Ti $2p_{1/2}$, and 457.2 eV corresponds to Ti $2p_{3/2}$ in the Ti 2p region (Figure 5a). The slitting between $Ti2p_{1/2}$ and Ti $2p_{3/2}$ is 5.9 eV which indicates the normal state of Ti^{4+} in the mesoporous anatase TiO_2. [71] The XPS peak (Figure 5b) at ~530 eV corresponds to the lattice oxygen of TiO_2 crystal and peaks at 532.1 and 531.7 eV correspond to the adsorbed oxygen on TiO_2 surface. Figure 5c shows the Ag $3d_{3/2}$ and Ag $3d_{5/2}$ peaks at the binding energy of 366.5 and 372.6 eV, respectively with a slitting of the 3d doublet of 6.1 eV, which suggest the zero valence silver instead of Ag^+ ions within the material. [72] So, the possible location of dopant is attributed as the surface or in the interstitial sites of the host material. The TEM or FE-SEM images confirm that there is no surface deposition of the silver on the particles. So, there is a fair possibility of the silver doping in the interstitial sites of the host material.

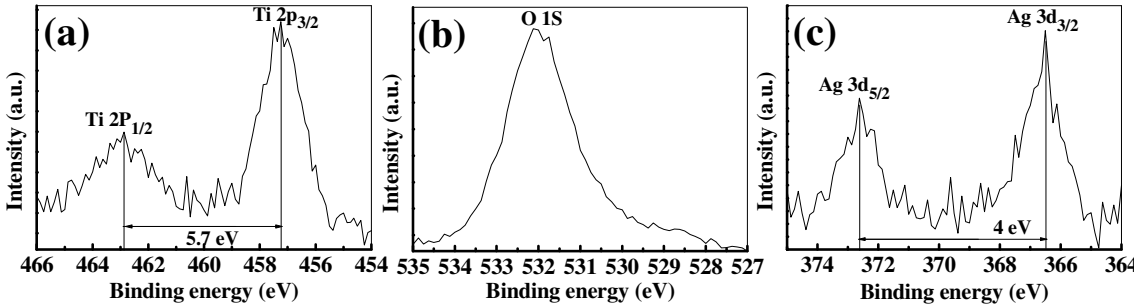

Figure 5. High resolution XPS narrow scan spectra of (a) Ti(2p), (b) O(1s), and (c) Ag(3d) for Ag-h-TiO_2 nanoparticles.

3.6 Characterization of particles by BET analysis

The specific surface area of the pure and hollow doped TiO_2 nanoparticles was measured by BET technique. Before the adsorption-desorption study the sample was degasified for 1 hr at 150°C temperature. The BET surface area of solid TiO_2 and Ag-h-TiO_2 nanoparticles are 95.1 and 198.3 m^2/g respectively. The Ag-h-TiO_2 nanoparticles are having 103.2 m^2/g more surface area compare to that of solid TiO_2. The obtained surface area of hollow structure TiO_2 is higher compared to the literature values of 38.9 - 123 m^2/g [62–66] This might be because of the core removal technique and the final particle size. In most of the literature the core was removed by calcinations but in our case the core is removed by dissolution at room temperature. The high surface area hollow structure TiO_2 is expected to be useful for the catalysis or other applications.

View Article Online
DOI: 10.1039/C5RA03421C

3.7 Photoluminescence activity of the synthesized nanoparticles

The photoluminescence (PL) properties of the synthesized nanoparticles were also checked by the fluorescence spectroscopy in terms of light emission. The light emission data was recorded between 500-600 nm wavelengths while excitation at 270 nm. The emission spectra of AgBr, TiO_2, AgBr/TiO_2, and Ag-h-TiO_2 NPs are presented in Figure 6. All the particles show emission in the visible region of wavelength ~ 543.8 nm. The intensities of emission are in the following order: AgBr > Ag-h-TiO_2 > AgBr/TiO_2 > TiO_2. The pure TiO_2 have very low intensity compared to pure AgBr and the intensity increases after the formation of Ag-h-TiO_2 NPs. The quantum yield (QY) was calculated for these materials from UV and PL data (Equation SI1, Supporting Information) using phenol as the standard material (QY = 0.14). The QYs of TiO_2, AgBr, AgBr/TiO_2, and Ag-h-TiO_2 NPs are 0.29, 0.498, 0.36, and 0.477 respectively. So, the quantum yield of TiO_2 is enhanced by 18.7% after the formation of hollow structure and Ag doping. From these results it can be pointed out that the Ag–h-TiO_2 nanoparticles has enhanced light emission property and QY compared to that of pure TiO_2 nanoparticles. So, the light emission properties along with the catalytic properties could be utilized for better photocatalyst or dye sensitized solar cells applications.

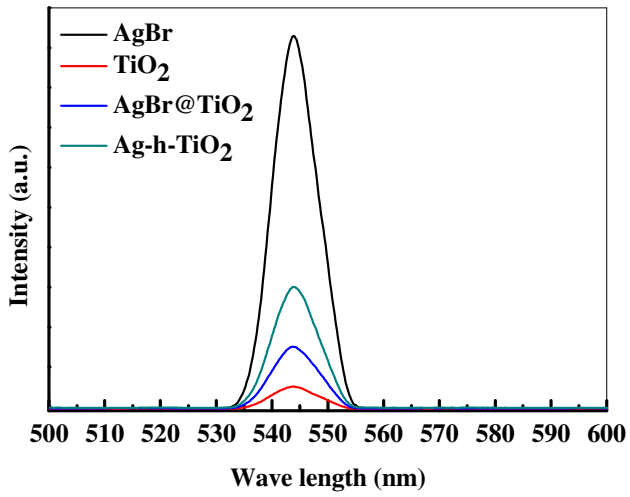

Figure 6. Light emission spectra of AgBr, TiO_2, AgBr/TiO_2, and Ag-h-TiO_2 NPs after excitation at 270 nm wavelength.

3.8 Photo catalytic applications of synthesized nanoparticles

View Article Online
DOI: 10.1039/C5RA03421C

The photocatalytic activities of the synthesized Ag-h-TiO_2 nanoparticles were first tested for the degradation of NB under the visible light irradiation. The degradation studies using pure and Ag doped solid TiO_2 (Ag-TiO_2) were also employed as the photocatalyst for the comparison purpose. The results of NB degradation in visible light are shown in Figure 7. It has been found that the degradation process reaches a plateau level after 3.5 hrs of light exposure time. The results show that at the plateau level, the degradation efficiencies of NB are 58.46, 89.61, and 95.5% in the presence of TiO_2, Ag-TiO_2, and Ag-h-TiO_2 NPs respectively. The results clearly indicate that the maximum degradation of the NB was obtained in the presence of the Ag-h-TiO_2 NPs. The degradation results were also fitted with different kinetic models, and it was found that the first order kinetics fits well for all the materials. The Figure 7b presents the reaction kinetics of NB degradation. The rate constants (k) of the photocatalytic degradation reactions obtained from the experimental results are 0.0045, 0.0109, and 0.016 min^{-1} for TiO_2, Ag-TiO_2, and Ag-h-TiO_2 NPs respectively. The rate constant of Ag-h-TiO_2 photocatalytic process is about 3.6 and 1.5 times than that of pure TiO_2 and Ag-TiO_2 photocatalytic processes respectively. A comparison at 50% degradation times for NB shows 136.5, 41.5, and 27 min for TiO_2, Ag-TiO_2, and Ag-h-TiO_2 nanoparticles, respectively. These results reveal that Ag-h-TiO_2 nanoparticles have higher photocatalytic activity compared to that of pure TiO_2 and Ag-TiO_2 NPs. This is attributed to the fact that pure TiO_2 is having low yield of $^{\bullet}OH$ radicals because of recombination of the charge carriers during photodegradation, which helps to oxidize the organic compound as stated in our previous study. [73] In Ag doped TiO_2 NPs the Ag dopant accepts the photoinduced electrons and holes, which in turn act as electron/hole traps and prevents the recombination of the charge carriers. In Ag-h-TiO_2 NPs, addition to Ag doping it is having more surface area (198.3 m^2/g as mentioned in the BET analysis) compared to solid TiO_2 (95.1 m^2/g), which is useful for better catalytic processes. Additionally, as mention in the XPS section, the presence of adsorbed oxygen on the TiO_2 surface allows the H^+ hydroxylation to form –Ti(OH)-O-Ti-(OH)- in the presence of water. During the photodegradation, this compound may help to generate the photogenerated hole (h^+_{VB}) and finally turn to $OH^{\bullet}$ free radicals, which is beneficial for the photocatalysis. [74] While comparing the degradation efficiency and PL intensity, it can be seen that Ag-h-TiO_2 is having high degradation efficiency as well as PL intensity compared to that of pure TiO_2. In general, high PL intensity is due to the high recombination of electrons and holes. Our results can be attributed in the following way. In the presence of doping, the reduction in

View Article Online
DOI: 10.1039/C5RA03421C

recombination continues up to the certain limit of doping percentage (optimum doping) and then again recombination starts increasing with the increasing doping %. [75,76] From the EDX study it is seen that 9.02% doping is achieved, which is higher compared to optimum doping percentage (1%) for TiO_2, [73] we beleive because of that the PL intensity is high. At the same time, as the surface area of hollow particles is higher than solid TiO_2, the degradation efficiency is more because of more adsorption of dye molecules. The reusability of Ag-h-TiO_2 NPs was tested by recycling the catalyst under the same condition, and the results are plotted in Figure 7c. The results show there is a ~10.83% decrease (95.5 to 84.67%) in degradation efficiency after sixth cycles. The turn over number (TON) of the photocatalyst is calculated as 0.467, 0.716, and 0.763 mol/mol for the first cycle of the TiO_2, Ag-TiO_2, Ag-h-TiO_2, respectively. From the reported literatures (Table S1, Supporting Information) it is has been found that more than 90% degradation efficiency of nitrobenzene was achieved either in the presence high catalyst dose, low organic concentration, in the presence of UV light irradiation, or in presence of some additives and at specific pH. In this regard, our catalytic process is more effective in normal visible light and in the absence of any additives than the already reported literatures.

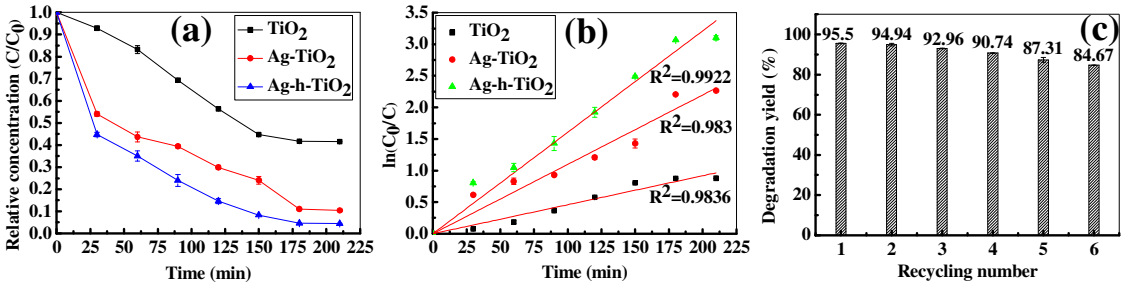

Figure 7. (a) Photodegradation kinetics of nitrobenzene under visible light of high pressure mercury vapour lamp using TiO_2, Ag-TiO_2 and Ag-h-TiO_2 NPs. (b) Fitting of first order kinetics with the experimental data. (c) Recycling test of Ag-h-TiO_2 for the degradation of nitrobenzene solution.

Further, to explore the degradation pathway of NB in the presence of TiO_2, Ag-TiO_2, and Ag-h-TiO_2 photocatalysts, LC-MS study was conducted to identify different photo degraded products. Based on the LC-MS results probable degradation path is proposed in Figure 8. During the photodegradation, the $^{\bullet}OH$ radicals attack the nitrobenzene and subsequently produce some aromatic compounds, such as benzene, phenol, catechol, resorcinol, and hydroquinone. The hydroquinone again forms benzoquinone through the dehydrogenation.

View Article Online
DOI: 10.1039/C5RA03421C

Further degradation of the aromatic compounds happens through the ring cleavage and some degraded product, such as propionic acid, n-butanol, di-ethyl ether, furan, orthoformic acid, propanol, and acetic acid are formed.

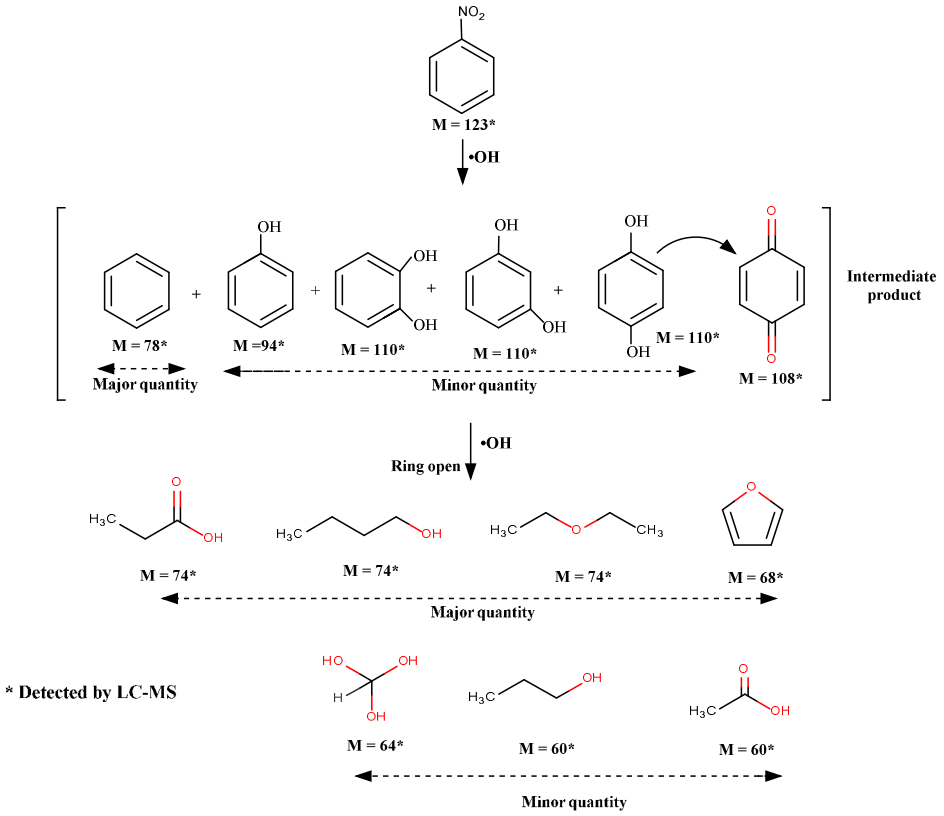

Figure 8. Probable pathway for the degradation of nitrobenzene under visible light in the presence of TiO_2, Ag-TiO_2, and Ag-h-TiO_2.

Since the Ag-h-TiO_2 nanoparticles show good photocatalytic degradation against the NB, the same catalyst was also used to study the photodegradation efficiency on other two classes of organic compounds such as metronidazole antibiotic and methylene blue dye under the visible light irradiation. The degradation results (Figure 9a) show that at the plateau level the degradation of MTZ is 96.55% in the presence of Ag-h-TiO_2 NPs, while pure TiO_2 and Ag-TiO_2 degraded 80.78 and 94.39% of MTZ. [73] The rate constant of the photocatalytic degradation reactions obtained from the experimental results is 0.0269 min^{-1} for Ag-h-TiO_2 NPs. The results of reusability test of Ag-h-TiO_2 NPs (Figure 9b) show there is a ~10.76% decrease (96.55 to 85.79%) in degradation efficiency after sixth cycles. It can be noted that the difference between hollow and solid TiO_2 is not significant (~2%), in spite of significantly high surface area for hollow particles, which can be attributed to the low initial

View Article Online
DOI: 10.1039/C5RA03421C

MTZ concentration. So, the initial concentration of MTZ was increased to 30 mg/L and it has been found that after 2 hrs the Ag-TiO_2 and Ag-h-TiO_2 NPs degraded 88.5 and 94.77% MTZ (Figure 9c) with rate constants 0.019 and 0.024 min^{-1} (Figure 9d) for Ag-TiO_2 and Ag-h-TiO_2 NPs respectively. These results indicate that, when the concentration of organic molecules is high hollow particles show better efficiency. Our approach of MTZ degradation is noble compared to the reported conventional method as well as photocatalytic degradation approach as discussed in the Supporting Information (Table S2). The surface chemistry of Ag-h-TiO_2 photocatalyst was studied before and after degradation of MTZ solution by FT-IR spectroscopy. The FT-IR results (Figure S3, Supporting Information) show there is no significant peak change between the virgin Ag-h-TiO_2 and recycled Ag-h-TiO_2 after degradation. The broad absorption peak at 3373 and 2359 cm^{-1} are associated with the asymmetric and symmetric stretching vibrations of the Ti–OH group. The peaks in the range 400-1000 cm^{-1} are the contribution of anatase phase Ti-O. So, these results strongly suggest that the degradation of MTZ solution is due to the photocatalytic degradation instead of any chemisorption or physisorption of MTZ on the catalyst surface.

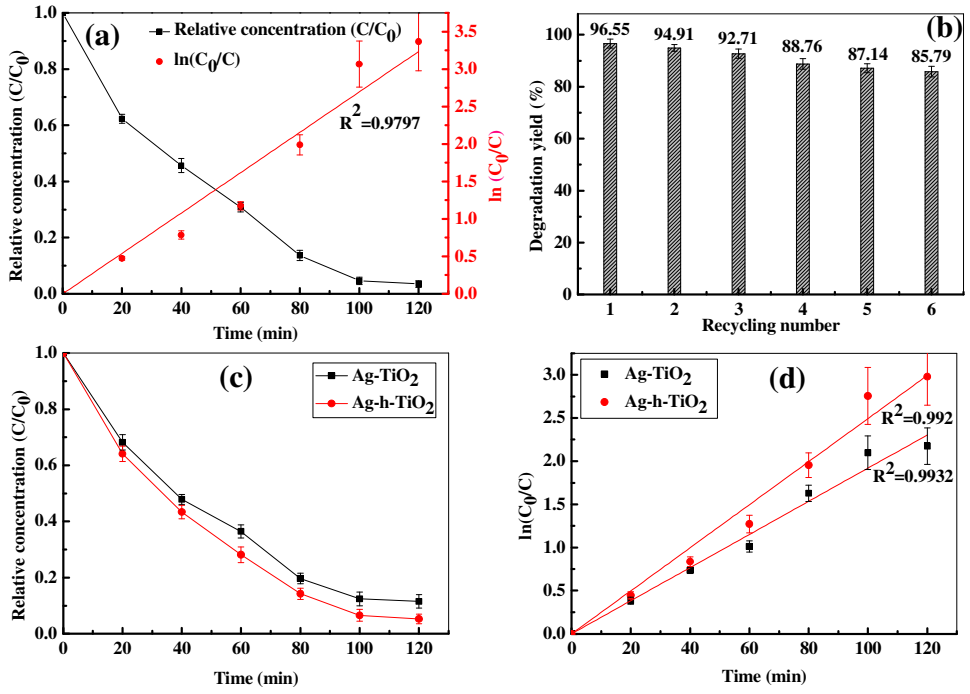

Figure 9. (a) Photodegradation kinetics and fitting of first order kinetics with the experimental data of MTZ degradation under visible light of high pressure mercury vapour lamp using Ag-h-TiO_2 NPs with 15 mg/L of initial MTZ concentration. (b) Recycling test of Ag-h-TiO_2 for the degradation of MTZ solution. (c) Photodegradation kinetics and (d) Fitting

View Article Online
DOI: 10.1039/C5RA03421C

of first order kinetics with the experimental data of MTZ using Ag-TiO_2 and Ag-h-TiO_2 NPs with 30 mg/L initial concentration of MTZ.

The MBD degradation was carried out under the visible light with 25 mg/L initial concentration of dye and the catalyst concentration of 0.25 g/L. The degradation results are presented in Figure S4, Supporting Information. The dye degradation efficiency of Ag-h-TiO_2 is 96.77 % after 3 hrs exposure time. The rate constant of photocatalytic degradation of MBD under the visible lamp using Ag-h-TiO_2 NPs is 0.0216 min^{-1} (Figure S4c, Supporting Information). Similar to previous study Ag-h-TiO_2 sample was further selected for cyclic degradation test under the same condition and found there is a decrease in efficiency of ~ 10.47% (96.77 to 86.3%) after sixth cycle of photodegradation (Figure S4d, Supporting Information).

For each type of organic compound degradation, two sets of reference studies, (i) organic solution + catalyst in dark and (ii) only organic solution under visible light irradiation were carried out. The first was to test only adsorption capacity. Since the catalyst concentration was low, there was no significant change found because of adsorption. So we confirmed that the concentration change was only because of degradation.

4. Conclusions

The hollow TiO_2 nanoparticles were synthesized by a sacrificial core method using AgBr as sacrificial core. During the removal of core, Ag was doped in the interstitial sites of the host TiO_2. The obtained Ag-h-TiO_2 nanoparticles are purely in anatase phase and good crystalline in nature. The mean particle size is 17.76 ± 2.85 nm with wall thickness of ~ 2.5 nm. The increase of surface area for hollow nanoparticles is 103.2 m^2/g more compared to that of solid TiO_2 nanopaticles. Apart from the surface area, the quantum yield of Ag-h-TiO_2 nanoparticles also increases to 18.7% compared to that of pure solid TiO_2 nanoparticles. The nanoparticles were used for the photo degradation of NB, MTZ antibiotic and MBD. The maximum NB degradation was obtained 95.5% under visible light irradiation for 3.5 hr. The metronidazole degradation efficiency was found to be 96.55 and 94.77% under the irradiation of visible light for the initial MTZ concentration of 15 and 30 mg/L with catalyst dose of 0.5 g/L. The Ag-h-TiO_2 NPs show only 10.47% decrease in degradation efficiency even after sixth cycle of reuse. The synthesized Ag-h-TiO_2 nanoparticles may also be useful for dye sensitized solar cells and other electrochemical applications.

Acknowledgments

View Article Online
DOI: 10.1039/C5RA03421C

The financial support from the Council of Scientific and Industrial Research (CSIR), Grant No. 22(0527)/10/EMR-II, for this project is gratefully acknowledged. S.S.B. thanks CSIR, India, for a Senior Research Fellowship to pursue this work. Authors are grateful to Indian Institute of Technology, Kharagpur, India, for providing their XPS facility. Authors also acknowledge the Saha Institute of Nuclear Physics, Indian Association for the Cultivation of Science, Kolkata, India, for giving the opportunity to access their TEM facility.

References

1. Liqiang, J.; Honggang, F.; Baiqi, W.; Dejun, W.; Baifu, X.; Shudan, L.; Jiazhong, S. Effects of Sn Dopant on the Photoinduced Charge Property and Photocatalytic Activity of TiO_2 Nanoparticles. *Appl. Catal., B: Environmental* **2006**, *62*, 282-291.
2. Zeng, H.; Cai, W.; Liu, P.; Xu, X.; Zhou, H.; Klingshirn, C.; Kalt, H. ZnO-Based Hollow Nanoparticles by Selective Etching: Elimination and Reconstruction of MetalSemiconductor Interface, Improvement of Blue Emission and Photocatalysis. ACS Nano **2008**, *2*, 1661-1670.
3. He, W.; Kim, H. k.; Wamer, W. G.; Melka, D.; Callahan, J. H. Photogenerated Charge Carriers and Reactive Oxygen Species in ZnO/Au Hybrid Nanostructures with Enhanced Photocatalytic and Antibacterial Activity. *J. Am. Chem. Soc.* **2014**, *136*, 750 - 757.
4. Jose, R.; Thavasi, V.; Ramakrishna, S. Metal Oxides for Dye-Sensitized Solar Cells. *J. Am. Ceram. Soc.* **2009**, *301*, 289-301.
5. Guo, J.; She, C.; Lian, T. Ultrafast Electron Transfer between Conjugated Polymer and Antimony-Doped Tin Oxide (ATO) Nanoparticles. *J. Phys. Chem. C* **2008**, *112*, 4761-4766.
6. Tubtimtae, A.; Arthayakul, K.; Teekwang, B.; Hongsith, K. MnTe Semiconductor-Sensitized Boron-Doped TiO_2 and ZnO Photoelectrodes for Solar Cell Applications. *J. Colloid Interface Sci.* **2013**, *405*, 78-84.
7. Reddy, A. L. M.; Shaijumon, M. M.; Gowda, S. R.; Ajayan, P. M. Coaxial MnO_2/Carbon Nanotube Array Electrodes for High-Performance Lithium Batteries. *Nano Lett.* **2009**, *9*, 1002-1006.
8. Chan, C. K.; Peng, H.; Twesten, R. D.; Jarausch, K. Zhang, X. F.; Cui, Y. Fast, Completely Reversible Li Insertion in Vanadium Pentoxide Nanoribbons. *Nano* Lett **2007**, *7*, 490-495.

View Article Online
DOI: 10.1039/C5RA03421C

9. Kimura, T., Dong, Q.; Yin, S.; Hashimoto, T.; Sasaki, A.; Sato, T. Synthesis and Piezoelectric Properties of Li-doped $BaTiO_3$ by a Solvothermal Approach. *J. Eur. Ceram. Soc.* **2013**, *33*, 1009-1015.

10. Yang, Q.; Guo, X.; Wang, W.; Zhang, Y.; Xu, S.; Lien, D. H.; Wang, Z. L. Enhancing Sensitivity of a Single ZnO Micro-/Nanowire Photodetector by Piezo-phototronic Effect. *ACS Nano* **2010**, *4*, 6285-6291.

11. Kamat, P.V. Graphene-Based Nanoarchitectures. Anchoring Semiconductor and Metal Nanoparticles on a Two-Dimensional Carbon Support. *J. Phys. Chem. Lett.* **2010**, *1*, 520–527.

12. Sun, Y. F.; Liu, S. B.; Meng, F. L.; Liu, J. Y.; Jin, Z.; Kong, L. T.; Liu, J. H. Metal Oxide Nanostructures and Their Gas Sensing Properties: A Review. *Sensors* **2012**, *12*, 2610-2631.

13. Hassan, H. S.; Kashyout, A. B.; Soliman, H. M. A.; Uosif, M. A.; Afify, N. Effect of reaction time and Sb doping ratios on the architecturing of ZnO nanomaterials for gas sensor applications. *Appl. Surf. Sci.* **2013**, *277*, 73-82.

14. Zaleska, A. Doped-TiO_2: A Review. *Rec. Patents Eng*. **2008**, *2*, 157-164.

15. Liu, Y.; Li, J.; Zhou, B.; Chen, H.; Wang, Z.; Cai, W. A TiO_2-Nanotube-Array-Based Photocatalytic Fuel Cell using Refractory Organic Compounds as Substrates for Electricity Generation. *Chem. Commun.* **2011**, *47*, 10314–10316.

16. Cao, S.; Yeung, K. L.; Yue, P. L. An Investigation of Trichloroethylene Photocatalytic Oxidation on Mesoporous Titania-Silica Aerogel Catalysts. *Appl. Catal., B: Environmental* **2007**, *76*, 64-72.

17. Zhu, J.; Chen, F.; Zhang, J.; Chen, H.; Anpo, M. Fe^{3+}-TiO_2 Photocatalysts Prepared by Combining Sol–gel Method with Hydrothermal Treatment and their Characterization. *J. Photochem. Photobiol., A: Chemistry* **2006**, *180*, 196-204.

18. Wang, W.; Zhang, J.; Chen, F.; He, D.; Anpo, M. Preparation and Photocatalytic Properties of Fe^{3+}-Doped Ag@TiO_2 Core–shell Nanoparticles. *J. colloid interface sci.* **2008**, *323*, 182-186.

19. Deng, Q. R.; Xia, X. H.; Guo, M. L.; Gao, Y.; Shao, G. Mn-doped TiO_2 Nanopowders with Remarkable Visible Light Photocatalytic Activity. *Mater. Lett.* **2011**, *65*, 2051-2054.

20. Behnajady, M. A.; Alizade, B.; Modirshahla, N. Synthesis of Mg-Doped TiO2 Nanoparticles under Different Conditions and its Photocatalytic Activity. *Photochem. photobiol.,* **2011**, *87*, 1308-1314.

View Article Online
DOI: 10.1039/C5RA03421C

21. Jaimy, K. B.; Ghosh, S.; Sankar, S.; Warrier, K. G. K. An Aqueous Sol–gel Synthesis of Chromium(III) Doped Mesoporous Titanium Dioxide for Visible Light Photocatalysis. *Mater. Res. Bull.* **2011**, *46*, 914-921.

22. Iwasaki, M.; Hara, M.; Kawada, H.; Tada, H.; Ito, S. Cobalt Ion-Doped TiO_2 Photocatalyst Response to Visible Light. *J. colloid interface sci.* **2000**, *224*, 202-204.

23. Kiraz, N.; Burunkaya, E.; Kesmez, Ö.; Çamurlu, H. E.; Asiltürk, M.; Yeşil, Z.;Arpaç, E. Preparation of Sn Doped Nanometric TiO_2 Powders by Reflux and Hydrothermal Syntheses and their Characterization. *J. Sol-Gel Sci. Technol.* **2011**, *59*, 381-386.

24. Xiao, Q.; Si, Z.; Yu, Z.; Qiu, G. Sol–gel Auto-combustion Synthesis of Samarium-Doped TiO2 Nanoparticles and their Photocatalytic Activity under Visible Light Irradiation. *Mater. Sci. Eng.: B* **2007**, *137*, 189-194.

25. Hewer, T. L. R.; Souza, E. C. C.; Martins, T. S.; Muccillo, E. N. S.; Freire, R. S. Influence of Neodymium Ions on Photocatalytic Activity of TiO_2 Synthesized by Sol–gel and Precipitation Methods. *J. Mol. Catal. A: Chemical* **2011**, *336*, 58-63.

26. Ji, L.; Wang, Z.; Li, Z.; Liang, J. Preparation of Aligned Titania Nanowires with an Aligned Carbon Nanotube Composite Template. *Mater. Lett.* **2008**, *62,* 1979-1982.

27. Grandcolas, M.; Ye, J.; Hanagata, N. Combination of Photocatalytic and Antibacterial Effects of Silver Oxide Loaded on Titania Nanotubes. *Mater. Lett.* **2011**, *65*, 236-239.

28. Zhang, Y.; Gao, Y.; Xia, X. H.; Deng, Q. R.; Guo, M. L.; Wan, L.; Shao, G. Structural Engineering of Thin Films of Vertically Aligned TiO_2 Nanorods. *Mater. Lett.* **2010**, *64*, 1614-1617.

29. Morey, M. S.; Bryan, J. D.; Schwarz, S.; Stucky, G. D. Pore Surface Functionalization of MCM-48 Mesoporous Silica with Tungsten and Molybdenum Metal Centers: Perspectives on Catalytic Peroxide Activation. *Chem. Mater.* **2000**, *12*, 3435-3444.

30. Okada, K.; Shimai, A.; Takei, T.; Hayashi, S.; Yasumori, A.; MacKenzie, K. J. D. Preparation of Microporous Silica From Metakaolinite by Selective Leaching Method. *Microporous Mesoporous Mater.* **1998**, *21*, 289-296.

31. Cochran, J. K. Ceramic Hollow Spheres and their Applications. *Curr. Opin. Solid State Mater. Sci.* **1998**, *3*, 474 –479.

32. Syoufian, A.; Inoue, Y.; Yada, M.; Nakashima, K. Preparation of Submicrometer-Sized Titania Hollow Spheres by Templating Sulfonated Polystyrene Latex Particles. *Mater. Lett.* **2007**, *61*, 1572-1575.

View Article Online
DOI: 10.1039/C5RA03421C

33. Cui, L.; Wang, Y.; Niu, M.; Chen, G.; Cheng, Y. Synthesis and visible light photocatalysis of Fe-doped TiO_2 mesoporous layers deposited on hollow glass microbeads. *J. Solid State Chem.* **2009**, *182*, 2785-2790.

34. Ma, G.; Jia, R.; Zhao, J.; Wang, Z.; Song, C.; Jia, S.; Zhu, Z. Nitrogen-Doped Hollow Carbon Nanoparticles with Excellent Oxygen Reduction Performances and Their Electrocatalytic Kinetics. *J. Phys. Chem. C* **2011**, *115*, 25148–25154.

35. Wang, C.; Ao, Y.; Wang, P.; Hou, J.; Qian, Preparation, Characterization and Photocatalytic Activity of the Neodymium-Doped TiO_2 Hollow Spheres *J. Appl. Surf. Sci.* **2010**, *257*, 227-231.

36. Wang, C.; Ao, Y.; Wang, P.; Hou, J.; Qian, J. Preparation of Cerium and Nitrogen Co-Doped Titania Hollow Spheres with Enhanced Visible Light Photocatalytic Performance. *Powder Technol.* **2011**, *210*, 203-207.

37. Wang, P.; Wu, J.; Ao, Y.; Wang, C.; Hou, J.; Qian, J. Preparation and Enhanced Photocatalytic Performance of Sn Ion Modifi ed Titania Hollow Spheres. *Mater. Lett.* **2011**, *65*, 3278-3280.

38. Xu, J.; Chen, M.; Fu, D. Study on Highly Visible Light Active Bi-Doped TiO_2 Composite Hollow Sphere. *Appl. Surf. Sci.* **2011**, *257*, 7381-7386.

39. An, G.; Yang, C.; Jin, S.; Chen, G.; Zhao, X. Hollow TiO_2:Sm3+ Spheres with Enhanced Photoluminescence Fabricated by a Facile Method using Polystyrene as Template. *J. Mater. Sci.* **2013**, *48*, 5483-5488.

40. Chaudhuri, R.G.; Paria, S. Visible Light Induced Photocatalytic Activity of Sulfur Doped Hollow TiO_2 Nanoparticles, Synthesized Via a Novel Route. *Dalton Trans.* **2014**, *43*, 5526-5534.

41. Awazu, K.; Fujimaki, M.; Rockstuhl, C.; Tominaga, J.; Murakami, H.; Ohki, Y.; Yoshida, N.; Watanabe, T. A Plasmonic Photocatalyst Consisting of Silver Nanoparticles Embedded in Titanium Dioxide. *J. Am. Chem. Soc.* **2008**, *130*, 1676-1680.

42. Tian, Y.; Tatsuma, T. Mechanisms and Applications of Plasmon-Induced Charge Separation at TiO_2 Films Loaded with Gold Nanoparticles. *J. Am. Chem. Soc.* **2005**, *127*, 7632-7637.

43. Sondi, I.; Salopek-Sondi, B. Silver Nanoparticles as Antimicrobial Agent: a Case Study on E. coli as a Model for Gram-negative Bacteria. *J. colloid interface sci.* **2004**, *275*, 177-182.

View Article Online
DOI: 10.1039/C5RA03421C

44. Smetana, A. B.; Klabunde, K. J.; Marchin, G. R.; Sorensen, C. M. Biocidal Activity of Nanocrystalline Silver Powders and Particles. *Langmuir* **2008**, *24*, 7457-7464.

45. Li, Q.; Mahendra, S.; Lyon, D. Y.; Brunet, L.; Liga, M. V.; Li, D.; Alvarez, P. J. J. Antimicrobial Nanomaterials for Water Disinfection and Microbial Control: Potential Applications and Implications. *Water research* **2008**, *42*, 4591-602.

46. Zhang, L.; Yu, J. C.; Yip, H. Y.; Li, Q.; Kwong, K. W. Ambient Light Reduction Strategy to Synthesize Silver Nanoparticles and Silver-Coated TiO_2 with Enhanced Photocatalytic and Bactericidal Activities. *Langmuir* **2003**, *19*, 10372-10380.

47. Guin, D.; Manorama, S. V.; Latha, J. N. L.; Singh, S. Photoreduction of Silver on Bare and Colloidal TiO_2 Nanoparticles/Nanotubes: Synthesis, Characterization, and Tested for Antibacterial Outcome. *J. Phys. Chem. C* **2007**, *111*, 13393-13397.

48. Xiang, Q.; Yu, J.; Cheng, B.; Ong, H. C. Microwave-Hydrothermal Preparation and Visible-Light Photoactivity of Plasmonic Photocatalyst Ag-TiO_2 Nanocomposite Hollow Spheres *Chem. Asian J.* **2010**, *5*, 1466 – 1474.

49. Song, C.; Wang, D.; Gu, G.; Lin, Y.; Yang, J.; Chen, L.; Fu, X.; Hu, Z. Preparation and Characterization of Silver/TiO_2 Composite Hollow Spheres. *J. colloid interface sci.* **2004**, *272*, 340-344.

50. Ji, P. L.; Kong, X. Z.; Wang, J. G.; Zhu, X. L. Characterization and Photocatalytic Properties of Silver and Silver Chloride Doped TiO_2 Hollow Nanoparticles. *Chin. Chem. Lett.* **2012**, *23*, 1399-1402.

51. Piccinini, P.; Minero, C.; Vincenti, M.; Pelizzetti, E. Photocatalytic Mineralization of Nitrogen-Containing Benzene Derivatives. *Catal. Today* **1997**, *39*, 187-195.

52. Bhatkhande, D. S.; Pangarkar, V. G.; Beenackers, A. A. C. M. Photocatalytic Degradation of Nitrobenzene using Titanium Dioxide and Concentrated Solar Radiation: Chemical Effects and Scaleup. *Water res.* **2003**, *37*, 1223-1230.

53. ElShafei, G. M. S.; Yehia, F. Z.; Dimitry, O. I. H.; Badawi, A. M.; Eshaq, G. Degradation of Nitrobenzene at Near Neutral pH using Fe^{2+} –Glutamate Complex as a Homogeneous Fenton Catalyst. *Appl. Catal., B: Environmental* **2010**, *99*, 242-247.

54. O'connor, O. A.; Young, L. Y. Toxicity and Anaerobic Biodegradability of Substituted Phenols under Methanogenic Conditions. *Environ. Toxicol. Chem.* **1989**, *8*, 853-862.

55. Zhao, L.; Ma, J.; Sun, Z. -z.; Zhai, X. -d. Catalytic Ozonation for the Degradation of Nitrobenzene in Aqueous Solution by Ceramic Honeycomb-Supported Manganese. *Appl. Catal., B: Environmental* **2008**, *83*, 256-264.

View Article Online
DOI: 10.1039/C5RA03421C

56. Elmolla, E. S.; Chaudhuri, M. Degradation of the Antibiotics Amoxicillin, Ampicillin and Cloxacillin in Aqueous Solution by the Photo-Fenton Process. *J. Hazard. Mater.* **2009**, *172*, 1476–1481.

57. Rysz, M.; Alvarez, P. J. J. Amplification and Attenuation of Tetracycline Resistance in Soil Bacteria: Aquifer Column Experiments. *Water Res.* **2004**, *38*, 3705–3712.

58. Gilliver, M. A.; Bennett, M.; Begon, M.; Hazel, S. M.; Hart, C. A. Enterobacteria: Antibiotic Resistance Found in Wild Rodents. *Nature* **1999**, *401*, 233–234.

59. Goni-Urriza, M.; Capdepuy, M.; Arpin, C.; Raymond, N.; Caumette, P.; Quentin, C. Impact of an Urban Effluent on Antibiotic Resistance of Riverine Enterobacteriaceae and Aeromonas spp. *Appl. Environ. Microbiol.* **2000**, *66*, 125–132.

60. Muruganandham, M.; Shobana, N.; Swaminathan, M. Optimization of Solar Photocatalytic Degradation Conditions of Reactive Yellow 14 Azo Dye in Aqueous TiO_2. *J. Mol. Catal. A* **2006**, *246*, 154–161.

61. Chun, H.; Yizhong, W. Decolorization and Biodegradability of Photocatalytic Treated Azo Dyes and Wool Textile Wastewater. *Chemosphere* **1999**, *39*, 2107-2115.

62. Guo, H.; Tian, D.; Liu, L.; Wang, Y.; Guo, Y.; Yang, X. Core–shell TiO_2 microsphere with enhanced photocatalytic activity and improved lithium storage. *J. Solid State Chem.* **2013**, *201*, 137-143.

63. Karan, N.S.; Agrawal, A.; Pandey, P. K.; Smitha, P.; Sharma, S. J.; Mishra, D. P.; Gajbhiye, N. S. Diffusion flame synthesis of hollow , anatase TiO_2 nanoparticles. *Mater. Sci. Eng., B* **2009**, *163,* 128–133.

64. Li, X.; Lv, K.; Deng, K.; Tang, J.; Su, R.; Sun, J.; Chen, L. Synthesis and characterization of ZnO and TiO_2 hollow spheres with enhanced photoreactivity. *Mater. Sci. Eng., B* **2009**, *158*, 40–47.

65. Song, C.; Yu, W.; Zhao, B.; Zhang, H.; Tang, C.; Sun, K.; Wu, X.; Dong, L.; Chen, Y. Efficient fabrication and photocatalytic properties of TiO_2 hollow spheres. *Catal. Commun.* **2009**, *10*, 650-654.

66. Zhang, F.; Zhang, Y.; Song, S.; Zhang, H. Superior electrode performance of mesoporous hollow TiO_2 microspheres through efficient hierarchical nanostructures. *J. Power Sources* **2011**, *196*, 8618-8624.

67. Ray, M. Paria, S. Growth Kinetics of Silver Bromide Nanoparticles in Aqueous Nonionic Surfactant Solutions. *Ind. Eng. Chem. Res.* **2011**, *50*, 11601-11607.

View Article Online
DOI: 10.1039/C5RA03421C

68. Hamal, D. B.; Klabunde, K. J. Synthesis, Characterization, and Visible Light Activity of new Nanoparticle Photocatalysts based on Silver, Carbon, and Sulfur-doped TiO_2. *J. colloid interface sci.* **2007**, *311*, 514-522.

69. Kawamura, G.; Sato, S.; Muto, H.; Sakai, M.; Lim, P. B.; Watanabe, K.; Inoue, M.; Matsuda, A. AgBr Nanocrystal-Dispersed Silsesquioxane– Titania hybrid Films for Holographic Materials. *Mater. Lett.* **2010**, *64*, 2648-2651.

70. Behnajady, M. A.; Eskandarloo, H.; Modirshahla, N.; Shokri, Investigation of the Effect of Sol – gel Synthesis Variables on Structural and Photocatalytic Properties of TiO_2 Nanoparticles. *Desalination* **2011**, *278*, 10-17.

71. Zhang, H.; Wang, G.; Chen, D.; Lv, X.; Li, J. Tuning Photoelectrochemical Performances of Ag-TiO_2 Nanocomposites via Reduction/Oxidation of Ag. *Chem. Mater.* **2008**, *20*, 6543–6549.

72. Du, J.; Zhang, J.; Liu, Z.; Han, B.; Jiang, T.; Huang, Y. Controlled Synthesis of Ag/TiO_2 Core-Shell Nanowires with Smooth and Bristled Surfaces via a One-Step Solution Route. *Langmuir* **2006**, *22*, 1307-1312.

73. Boxi, S. S.; Paria, S. Effect of Silver Doping on TiO_2, CdS, and ZnS Nanoparticles for the Photocatalytic Degradation of Metronidazole under Visible Light. *RSC Adv.* **2014**, *4*, 37752-37760.

74. Hoffmann, M. R.; Martin, S. T.; Choi, W.; Bahnemannt, D. W. Environmental Applications of Semiconductor Photocatalysis. *Chem. Rev.* **1995**, *95*, 69-96.

75. Choi, W.; Termin, A.; Hoffmann, M. R. The Role of Metal Ion Dopants in Quantum-Sized TiO_2: Correlation between Photoreactivity and Charge Carrier Recombination Dynamics. *J. Phys. Chem.* **1994**, *98*, 13669-13679.

76. Liqiang, J.; Honggang, F.; Baiqi, W.; Dejun, W.; Baifu, X.; Shudan, L.; Jiazhong, S. *Appl. Catal. B: Environmental* **2006**, *62*, 282-291.